2013 IEEE International Conference on Robotics and Automation (ICRA)
Karlsruhe, Germany, May 6-10, 2013

Speed Regulation in 3D Robotic Walking through Motion Transitions between Human-Inspired Partial Hybrid Zero Dynamics

Matthew J. Powell, Ayonga Hereid, and Aaron D. Ames

Abstract— **This paper employs the Human-Inspired Control framework in the formal design, optimization and implementation of controllers for 3D bipedal robotic walking. In this framework, controllers drive the robot to a low-dimensional representation, termed the partial hybrid zero dynamics, which is shaped by the parameters of the outputs describing human locomotion data. The main result of this paper is the use of partial hybrid zero dynamics in an optimization problem to compute physical constraints on the robot, without integrating the dynamics of the system, and while simultaneously yielding provably stable walking controllers for a 3D robot model. Controllers corresponding to various walking speeds are obtained through a second speed regulation optimization, and formal methods are presented which provide smooth transitions between walking speeds. These formal results are demonstrated through simulation and utilized to obtain 3D walking experimentally with the NAO robot.**

I. Introduction

Three-dimensional bipedal robotic walking has been realized experimentally by numerous robotic systems through the use of various control schemes[1]. One of the most prevalent control approaches leverages the Zero Moment Point (ZMP) [2], [3], which is the control scheme included as the default walking for the NAO[1] robot platform used as a testbed for the controllers designed in this work. From a purely mechanical point of view, passive walkers [4] employ an excellent understanding of mechanics and mechanism design to experimentally achieve robotic walking down small slopes without the use of control. These ideas have been used to design passivity-based control laws in 2D [5], [6]. These 2D control laws have been extended to 3D through geometric reduction [7], [8], yet these methods have only recently been realized experimentally [9]. Therefore, there exists a gap between formal methods and experimental realization for three-dimensional robotic walking. The goal of this work is to begin the process of bridging this gap by providing formal results that provably result in robotic walking which can be realized in experimentation.

The main idea behind this work is to approach 3D robotic walking through reductions based upon virtual models and constraints to create a low-dimensional representation of a bipedal robot that allows formal properties of the robot to be proven in a computationally tractable fashion. Low-dimensional representations have been studied before; see, for example, [10]. Similar ideas have been considered in the past through Hybrid Zero Dynamics [11], [12] (which has recently been applied to 3D robots [7]) and the spring-loaded inverted pendulum [13], [14], or SLIP model. Differing from traditional approaches, the authors' previous results [15], [16] show that certain outputs of the human locomotion control system can be represented by the solution to an under-damped, second-order mass-spring-damper system, and employed to achieve walking for a 2D robot model of NAO. Novel to this paper is the application of the human-inspired control framework to a 3D robot model of NAO, with computation of constraints necessary to physically realize walking on the actual robot.

This paper proposes a formal *human-inspired optimization* (HIO) which provably results in exponentially stable bipedal robotic walking *and* satisfies many of the physical constraints necessary to realize the walking experimentally. Specifically, the optimization minimizes an objective function which is the least-squares fit of the output functions of the robot to the human output data. Constraints are enforced which guarantee that the zero dynamics surface associated with the certain output functions is invariant through impact resulting in a *partial hybrid zero dynamics* [15]. These constraints, together with a specific choice of (linear) output functions, allow for a closed-form approximation of the solution to the dynamics of the robot over the course of one step, i.e., the behavior of the robot can be determined *without integrating the dynamics of the system.* This allows for the computation of physical constraints required for experimental implementation, such as the ZMP and friction, to be added to the HIO as constraints and computed in a feasible time-frame (as opposed to the time required to integrate the full dynamics of the system, which in the case of the robot model considered in this paper is 20-dimensional).

In addition to walking at a constant speed, formal methods are presented for obtaining walking at multiple speeds through *speed regulation*—in the form of another optimization which yields controllers corresponding to a partial hybrid zero dynamics surface for each walking speed. *Motion Transitions* are constructed to smoothly connect two partial hybrid zero dynamics surfaces. Specifically, parameters of the *extended canonical walking function* are obtained through closed form expressions which satisfy PHZD at the beginning and end of the step. These motion transitions allow for seamless regulation of the robot's walking speed, and as a result, provide the ability to quickly change the robot's walking speed, as presented in the final section on simulation and experimental results.

M. J. Powell, A. Hereid and A. D. Ames are with the Department of Mechanical Engineering, Texas A&M University, College Station, TX 77843, e-mail: {mjpowell,ayonga,aames}@tamu.edu

This research is supported by NASA grant NNX11AN06H, NSF grants CNS-0953823 and CNS-1136104, and NHARP award 00512-0184-2009.

[1] http://www.aldebaran-robotics.com/

II. Robot Model

The NAO robot can be modeled as a hybrid control system:

$$\mathscr{HC}^R = (\mathcal{D}^R, U^R, S^R, \Delta^R, f^R, g^R). \tag{1}$$

Restrictions are imposed via control which render both feet flat throughout the gait; for non flat-foot models, more complex hybrid systems must be considered [7], [8]. The configuration space, $\mathcal{Q}^R$, of the system is given in coordinates by:

$$q = (\varphi_{sa}, \theta_{sa}, \theta_{sk}, \theta_{sh}, \varphi_{sh}, \varphi_{nsh}, \theta_{nsh}, \theta_{nsk}, \theta_{nsa}, \varphi_{nsa})^T,$$

where, as illustrated in Figure 1, φ_{sa}, φ_{sh}, φ_{nsh}, and φ_{nsa} are the stance ankle, stance hip, nonstance hip and nonstance ankle roll angles, respectively, and θ_{sa}, θ_{sk}, θ_{sh}, θ_{nsh}, θ_{nsk}, and θ_{nsa} are the stance ankle, stance knee, stance hip, nonstance hip, nonstance knee and nonstance ankle pitch angles, respectively. Note that the configuration is the 3D version of the commonly employed seven-link biped model [17], [1]. With the mass, length and inertia properties of each link of the robot, the Lagrangian can be computed which, through the Euler-Lagrange equation (see [18]), yields the equations of motion which can be converted to a set of first order ordinary differential equations (ODEs) resulting in the affine control system (f^R, g^R):

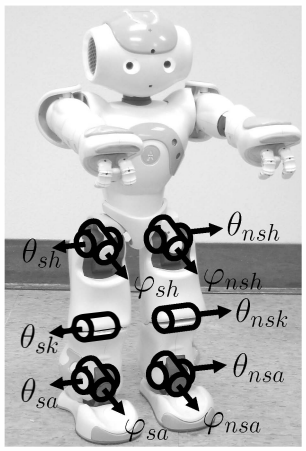

Fig. 1: Angle conventions for NAO.

$$f^R(q,\dot{q}) = \begin{bmatrix} \dot{q} \\ -D^{-1}(q)H(q,\dot{q}) \end{bmatrix}, g^R(q) = \begin{bmatrix} \mathbf{0} \\ D^{-1}(q)B(q) \end{bmatrix},$$

with $U^R \subseteq \mathbb{R}^{10}$ and $B : \mathcal{Q}^R \to \mathbb{R}^{10\times 10}$. For the choice of coordinates in this paper, $B = I_{10}$. The domain specifies the allowable configuration of the system, determined by a unilateral constraint $h^R : \mathcal{Q}^R \to \mathbb{R}$; for the biped considered in this paper, this function is the height of the non-stance foot. In particular, the domain and guard are given by:

$$\begin{aligned} \mathcal{D}^R &= \left\{(q,\dot{q}) \in T\mathcal{Q}^R : h^R(q) \geq 0\right\}. \\ S^R &= \left\{(q,\dot{q}) \in T\mathcal{Q}^R : h^R(q) = 0 \text{ and } dh^R(q)\dot{q} < 0\right\}, \end{aligned} \tag{2}$$

where $dh^R(q)$ is the Jacobian of h^R at q. The reset map $\Delta^R : S^R \to \mathcal{D}^R$ is given by:

$$\Delta^R(q,\dot{q}) = \begin{bmatrix} \Delta_q q \\ \Delta_{\dot{q}}(q)\,\dot{q} \end{bmatrix}, \tag{3}$$

where Δ_q is the relabeling matrix which switches the stance and non-stance legs at impact (by appropriately changing the angles). Here, $\Delta_{\dot{q}}$ determines the change in velocity due to impact (see [19], [7] and [15]).

III. Human-Inspired Controller Design

In the authors' previous work [15], it was shown that certain outputs of human locomotion, computed from experimental locomotion data, can each be represented by a function termed the *canonical walking function (CWF)*:

$$y_H(t,\alpha) = e^{-\alpha_4 t}(\alpha_1 \cos(\alpha_2 t) + \alpha_3 \sin(\alpha_2 t)) + \alpha_5. \tag{4}$$

Motivated by the desire to obtain human-like, bipedal robotic locomotion, the goal is to construct a controller which drives outputs of the robot to outputs of the human. This goal is effected formally through a control law $u : T\mathcal{Q}^R \to U^R$ which guarantees that $y^a(q(t)) \to y^d(t)$ exponentially as $t \to \infty$, where $y^a : \mathcal{Q}^R \to \mathbb{R}^{10}$ is a vector of kinematics maps on the robot representing the human outputs and $y^d : \mathbb{R} \to \mathbb{R}^{10}$ is a vector of canonical human functions.

With the goal of controlling the robot's walking speed, define the relative degree 1 actual output as the velocity of the hip and define the desired velocity of the hip:

$$y_1^a(q,\dot{q}) = \delta\dot{p}^R_{\text{hip}}(q,\dot{q}) = d\delta p^R_{\text{hip}}(q)\dot{q}, \qquad y_1^d = v_{\text{hip}}, \tag{5}$$

where $\delta p_{\text{hip}}(q)$ is the linearized position of the hip, given by

$$\delta p^R_{\text{hip}}(q) = L_c(-\theta_{sa}) + L_t(-\theta_{sa} - \theta_{sk}). \tag{6}$$

Furthermore, define the linear (relative degree 2) actual human outputs and desired outputs represented by the walking functions:

$$y^a_{2,L}(q) = \begin{bmatrix} \delta m^R_{nsl}(q) \\ \theta_{sk} \\ \theta_{nsk} \\ \theta^R_{tor}(q) \\ \varphi_{sa} \\ \varphi_{sh} \\ \varphi_{nsh} \end{bmatrix}, \; y^d_{2,L}(t,\alpha) = \begin{bmatrix} y_H(t,\alpha_{nsl}) \\ y_H(t,\alpha_{sk}) \\ y_H(t,\alpha_{nsk}) \\ y_H(t,\alpha_{tor}) \\ y_H(t,\alpha_{sa}) \\ y_H(t,\alpha_{sh}) \\ y_H(t,\alpha_{nsh}) \end{bmatrix} \tag{7}$$

where $y^a_{2,L} : \mathcal{Q}^R \to \mathbb{R}^7$ are the actual linear outputs of the robot, and $y^d_{2,L} : \mathbb{R} \times \mathbb{R}^{35} \to \mathbb{R}^7$ are the desired functions for these linear outputs, $\theta^R_{tor}(q) = \theta_{sa} + \theta_{sk} + \theta_{sh}$, and

$$\delta m^R_{nsl}(q) = -\theta_{sa} - \theta_{sk} - \theta_{sh} - \theta_{nsh} + \frac{L_c}{L_c + L_t}\theta_{nsk}. \tag{8}$$

The first four outputs of (7) were used to obtain walking in a 2D model of this system [16]; the three additional outputs $\varphi_{sa}, \varphi_{sh}, \varphi_{nsh}$ corresponding to the roll angles are novel to this work. Due to the linear form of the outputs considered, they can be written as:

$$y^a_{2,L}(q) = H\,q \tag{9}$$

for $H \in \mathbb{R}^{7\times 8}$ with full row rank (where, for example, the top row of H is obtained by taking the Jacobian of (8) with respect to the first 8 angles of the system). To enforce a flat non-stance foot and complete the set of controller outputs, two nonlinear, relative degree two outputs are needed:

$$y^a_{2,N}(q) = \begin{bmatrix} \psi^R_x \\ \psi^R_y \end{bmatrix}, \; y^d_{2,N}(t,\alpha) = \begin{bmatrix} \psi^d_x(t,\alpha_{\psi x}) \\ \psi^d_y(t,\alpha_{\psi y}) \end{bmatrix}, \tag{10}$$

where ψ_x^R and ψ_y^R represent the roll and pitch angles of the non-stance foot frame with respect to the ground frame. Grouping the linear and nonlinear relative degree two outputs results in:

$$y_2^a(q) = \begin{bmatrix} y_{2,L}^a(q) \\ y_{2,N}^a(q) \end{bmatrix}, \; y_2^d(t,\alpha) = \begin{bmatrix} y_{2,L}^d(t,\alpha) \\ y_{2,N}^d(t,\alpha) \end{bmatrix}. \quad (11)$$

where the parameters of all of the outputs are combined to yield a single vector $\alpha \in \mathbb{R}^{46}$ given by:

$$\alpha = (v_{\text{hip}}, \alpha_{nsl}, \alpha_{sk}, \alpha_{nsk}, \alpha_{tor}, \alpha_{sa}, \alpha_{sh}, \alpha_{nsh}, \alpha_{\psi x}, \alpha_{\psi y}).$$

The goal is for the outputs of the robot to agree with the outputs of the human, motivating the final form of the outputs to be used in feedback linearization:

$$y_1(q,\dot{q},\alpha) = y_1^a(q,\dot{q}) - v_{hip}, \quad (12)$$

$$y_2(q,\alpha) = y_2^a(q) - y_2^d(\tau(q),\alpha), \quad (13)$$

where $\tau(q) = \frac{\delta p_{\text{hip}}^R(q) - \delta p_{\text{hip}}^R(q^+)}{v_{\text{hip}}}$ is a state-based parameterization of time with $\delta p_{\text{hip}}^R(q^+)$ the linearized position of the hip of the robot at the beginning of a step. This parameterization is important as it allows for control over walking speed through the parameter v_{hip}. These outputs can be used to define a *human-inspired controller*:

$$u_{\alpha,\varepsilon}(q,\dot{q}) = \mathcal{A}(q,\dot{q})^{-1}\left(\begin{bmatrix} 0 \\ L_{f^R}^2 y_2(q,\dot{q}) \end{bmatrix} + \begin{bmatrix} L_{f^R} y_1(q,\dot{q}) \\ 2\varepsilon L_{f^R} y_2(q,\dot{q}) \end{bmatrix} + \begin{bmatrix} \varepsilon y_1(q,\dot{q}) \\ \varepsilon^2 y_2(q) \end{bmatrix}\right), \quad (14)$$

with control gain ε and decoupling matrix $\mathcal{A}$ given by

$$\mathcal{A}(q,\dot{q}) = \begin{bmatrix} L_{g^R} y_1(q,\dot{q},\alpha) \\ L_{g^R} L_{f^R} y_2(q,\dot{q},\alpha) \end{bmatrix} \quad (15)$$

and it follows that for a control gain $\varepsilon > 0$, the control law $u_{\alpha,\varepsilon} : T\mathcal{Q}^R \times \mathbb{R}^{46} \times \mathbb{R}^+ \to U^R$ renders the output exponentially stable [20].

For the hybrid control system $\mathscr{HC}^R$, the human-inspired control law is applied to obtain the hybrid system

$$\mathscr{H}_{\alpha,\varepsilon}^R = (\mathcal{D}^R, S^R, \Delta^R, f_{\alpha,\varepsilon}^R) \quad (16)$$

with $f_{\alpha,\varepsilon}^R(q,\dot{q}) = f^R(q,\dot{q}) + g^R(q,\dot{q})u_{\alpha,\varepsilon}(q,\dot{q})$. The end result of the modeling process is a hybrid system $\mathscr{H}_{\alpha,\varepsilon}^R$ that depends on the parameters of the human inspired control α and ε.

Hybrid Zero Dynamics For the *continuous* dynamics of the hybrid system $\mathscr{H}_{(\alpha,\varepsilon)}^R$, the controller renders the *full zero dynamics surface*

$$\mathbf{FZ}_\alpha = \left\{(q,\dot{q}) \in T\mathcal{Q}^R : y_1(q,\alpha) = 0, y_2(q,\dot{q},\alpha) = \mathbf{0}_9, \; L_{f^R} y_2(q,\dot{q},\alpha) = \mathbf{0}_9\right\}, \quad (17)$$

exponentially stable (where $\mathbf{0}_n$ is a vector of n zeros). In this work, hybrid invariance is enforced only for the relative degree 2 outputs. The corresponding surface is referred to as the *partial zero dynamics surface (PHZD)*:

$$\mathbf{PZ}_\alpha = \left\{(q,\dot{q}) \in T\mathcal{Q}^R : y_2(q,\alpha) = \mathbf{0}_9, \; \dot{y}_2(q,\dot{q},\alpha) = \mathbf{0}_9\right\}. \quad (18)$$

Since the only output that is not included in the partial zero dynamics surface is the output that forces the forward hip velocity to be constant, enforcing partial hybrid zero dynamics means, in some respect, that the velocity of the hip is allowed to compensate for the shocks in the system due to impact.

IV. Human-Inspired Controller Optimization

This section presents the main result of this paper: an optimization problem which yields parameters for the human-inspired controller, $u_{\alpha,\varepsilon}$, that minimize a human data-based cost function [21] while simultaneously yielding robotic walking in simulation and satisfying physical modeling constraints of the actual robot. A novel method is presented for computing these constraints in closed form (rather than explicitly integrating the dynamics) through the interplay between full and partial hybrid zero dynamics.

Optimization Cost. The cost of the optimization is the least squares fit of the sagittal plane outputs to the corresponding mean human data. The mean human data consist of discrete times, $t^H[k]$, and discrete values for the output functions: $\delta p_{\text{hip}}^H[k]$, $\delta m_{nsl}^H[k]$, $\theta_{sk}^H[k]$, $\theta_{nsk}^H[k]$, and $\theta_{tor}^H[k]$ where here $k \in \{1,\dots,K\} \subset \mathbb{N}$ with K the number of data points. Represent the mean human output data by $y_i^H[k]$ and the canonical walking functions by $y_i^d(t,\alpha_i)$ for $i \in \text{Output} = \{hip, msl, sk, nsk, tor\}$; for example, $y_{msl}^H[k] = \delta m_{nsl}^H[k]$ and $y_{msl}^d(t,\alpha_{msl}) = \delta m_{nsl}^d(t,\alpha_{nsl})$. With these elements defined, the human data based cost can be written

$$\text{Cost}_{\text{HD}}(\alpha) = \sum_{k=1}^{K} \sum_{i \in \text{Output}} \left(y_i^H[k] - y_i^d(t^H[k],\alpha_i)\right)^2, \quad (19)$$

which is simply the sum of squared residuals.

Partial Hybrid Zero Dynamics Constraints Following from [15], [16], to compute the constraints needed to ensure *partial hybrid zero dynamics*, the outputs and guard functions are used to explicitly solve for the configuration of the system $\vartheta(\alpha) \in \mathcal{Q}^R$ on the guard ($h^R(\vartheta(\alpha)) = 0$) in terms of the parameters α. In particular, let

$$\vartheta(\alpha) = q \quad \text{s.t.} \quad y_2(\Delta_q q) = \mathbf{0}_9 \;\text{ and }\; h^R(q) = 0 \quad (20)$$

where Δ_q is the relabeling matrix (3). Note that multiple solutions to $\vartheta(\alpha)$ exist because $y_{2,N}^d(\Delta_q q)$ and $h^R(q)$ are nonlinear functions of all joint angles; however, restrictions are placed on $\vartheta(\alpha)$ such that only one solution corresponds to a valid configuration. Using $\vartheta(\alpha)$ allows for the explicit solution of a point $(\vartheta(\alpha), \dot{\vartheta}(\alpha)) \in \mathbf{FZ}_\alpha \cap S^R$. In particular, let

$$Y(q) = \begin{bmatrix} d\delta p_{\text{hip}}^R(q) \\ dy_2(q) \end{bmatrix}. \quad (21)$$

and define

$$\dot{\vartheta}(\alpha) = Y^{-1}(\vartheta(\alpha)) \begin{bmatrix} v_{\text{hip}} \\ \mathbf{0}_9 \end{bmatrix}, \quad (22)$$

where Y is invertible because of the choice of outputs. Utilizing these constructions, the constraints needed for partial hybrid zero dynamics can be written:

$$y_2(\vartheta(\alpha)) = \mathbf{0}_9, \tag{C1}$$
$$dy_2(\Delta_q\vartheta(\alpha))\Delta_{\dot{q}}(\vartheta(\alpha))\dot{\vartheta}(\alpha) = \mathbf{0}_9, \tag{C2}$$
$$dh^R(\vartheta(\alpha))\dot{\vartheta}(\alpha) < 0. \tag{C3}$$

Computing approximate solutions: $q^e(t,\alpha)$ and $\dot{q}^e(t,\alpha)$ This section utilizes the fact that the human outputs were specifically chosen to be linear in order to explicitly construct the *partial hybrid zero dynamics*. Because of the specific choice of $y^a_{2,L}$, the following representation of the partial zero dynamic coordinates is employed:

$$\begin{aligned} \xi_1 &= \delta p^R_{\text{hip}}(q) =: c\,q, \\ \xi_2 &= y^a_1(q,\dot{q}) = \delta \dot{p}^R_{\text{hip}}(q,\dot{q}) =: c\,\dot{q}. \end{aligned} \tag{23}$$

where $c \in \mathbb{R}^{1\times 8}$ is obtained from (6). This motivates the following time-based approximation of ξ_1 and ξ_2 (utilizing the solution to the inverse kinematics):

$$\begin{aligned} \xi^e_1(t) &:= v_{\text{hip}}t + \delta p^R_{\text{hip}}(\Delta_q\vartheta(\alpha)), \\ \xi^e_2(t) &:= v_{\text{hip}}. \end{aligned} \tag{24}$$

These time-based approximations can be used in the partial zero dynamics surface to obtain an approximation of the solution for the full-order system by picking the coordinates

$$\begin{aligned} \eta_1 &= y^a_{2,L}(q) = H\,q, \\ \eta_2 &= L_{f_\mathcal{R}} y^a_{2,L}(q,\dot{q}) = H\,\dot{q}, \end{aligned} \tag{25}$$

with H as in (9), and defining

$$\Phi(\xi_1,\alpha) = \begin{bmatrix} c \\ H \end{bmatrix}^{-1} \begin{pmatrix} \xi_1 \\ y^d_{2,L}(\xi_1,\alpha) \end{pmatrix}, \tag{26}$$

$$\Psi(\xi_1,\alpha) = \begin{bmatrix} c \\ H \end{bmatrix}^{-1} \begin{pmatrix} 1 \\ \frac{\partial y^d_{2,L}(\xi_1,\alpha)}{\partial \xi_1} \end{pmatrix}. \tag{27}$$

yields estimates of the first eight angles and corresponding velocities of the system:

$$q^e_{1:8}(t,\alpha) = \Phi(\xi^e_1(t),\alpha), \tag{28}$$
$$\dot{q}^e_{1:8}(t,\alpha) = \Psi(\xi^e_1(t),\alpha)\xi^e_2(t). \tag{29}$$

The final four states of the system, $(q^e_{9:10}, \dot{q}^e_{9:10}) = (\theta^e_{nsa}, \varphi^e_{nsa}, \dot{\theta}^e_{nsa}, \dot{\varphi}^e_{nsa})^T$, are obtained through inverse kinematics with the assumption that the non-stance foot is parallel to the ground throughout the step.

Model Constraints Standard methods [7] are used to compute the ground contact forces and torques acting on the stance foot: $F_{st} = (F^{fx}_{st}, F^{fy}_{st}, F^{fz}_{st}, F^{mx}_{st}, F^{my}_{st}, F^{mz}_{st})$, where the first three components are the forces and the last three components are the torques acting on the stance foot. To prevent rotation about an edge, the following constraints on the ground reaction moment must hold [22]:

$$-\frac{w_f}{2}F^{fz}_{st} < F^{mx}_{st} < \frac{w_f}{2}F^{fz}_{st} \tag{30}$$
$$-l_h F^{fz}_{st} < F^{my}_{st} < l_t F^{fz}_{st}, \tag{31}$$

where w_f is the width of the foot, l_t is the length of the toe and l_h is the length of the heel. This condition is known as the Zero Moment Point condition [2], [3]. Furthermore, to prevent the stance foot from slipping, the following constraint must hold:

$$\sqrt{(F^{fx}_{st})^2 + (F^{fy}_{st})^2} < \mu F^{fz}_{st}, \tag{32}$$

where μ is the coefficient of static friction for the contact between NAO's foot and the ground. Equations (30)-(32) can be rearranged and stated in terms of inequalities of the form $C_i(u) < 0$ for $i \in \{1,\dots,5\}$. Moreover, using the approximation to the solution, $(q^e(t,\alpha), \dot{q}^e(t,\alpha))$, an approximation the torque is computed at each time, t, over the course of a step:

$$u^e_{\alpha,\varepsilon}(t) := u_{\alpha,\varepsilon}(q^e(t,\alpha), \dot{q}^e(t,\alpha)). \tag{33}$$

Therefore, the ZMP and friction constraints on the stance foot can be stated as the constraint:

$$\max_{i\in\{1,\dots,5\}} \max_{t\in[0,\tau(\vartheta(\alpha))]} C_i(u^e_{\alpha,\varepsilon}(t)) < 0, \tag{C4}$$

where $\tau(\vartheta(\alpha))$ provides an approximation of the duration of a step (and will converge to the actual step time as $\varepsilon \to \infty$).

The nonstance foot is kept parallel to the ground via control, through the following constraints on α:

$$\alpha_{\psi x} = \mathbf{0}_{1\times 5}, \qquad \alpha_{\psi y} = \mathbf{0}_{1\times 5}. \tag{C5}$$

These constraints on $\alpha_{\psi x}$ and $\alpha_{\psi y}$ reduce the size of the optimization search space to $\mathbb{R}^{36}$.

Optimization Problem Statement. The goal of *human-inspired PHZD optimization* is to find parameters α^* which solve the following constrained optimization problem:

$$\begin{aligned} \alpha^* = \underset{\alpha\in\mathbb{R}^{46}}{\text{argmin}} \ & \text{Cost}_{\text{HD}}(\alpha) \\ \text{s.t.} \ & \text{(C1)} - \text{(C5)} \end{aligned} \tag{HIO}$$

with Cost_{HD} the cost given in (19). The main result of this paper is established by combining the constructions and results of this section with Theorem 2 of [16]. It particular, it establishes that solving this optimization problem results in a exponentially stable periodic orbit for $\mathscr{H}^R_{\alpha^*,\varepsilon}$ (see [16] for a formal definition of solutions, and the corresponding definitions of periodic solutions and exponentially stable periodic orbits). Furthermore, physically realistic robotic walking can be ensured *without integrating the dynamics*.

V. Walking Speed Regulation

The solution, α^*, of the optimization problem (HIO) corresponds to a partial zero dynamics surface, $\mathbf{PZ}^*_\alpha$, and specifies controller outputs for walking at constant speed v^*_{hip}. However, as robotic locomotion is not always performed at a constant speed, controllers which provide the ability to smoothly transition between slow and fast walking are essential for functional robot operation. Here, a novel method for transitioning between these different walking speeds is presented; specifically, through the use of the *extended canonical walking function*, we will connect the

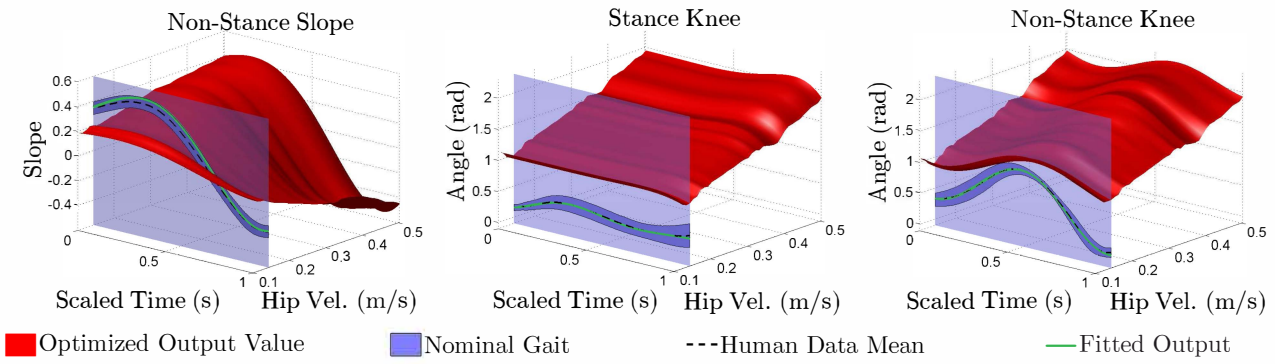

Fig. 2: Optimization for 80 values of v_{hip} and comparison to human data. The fitted outputs represents the canonical walking function fit to the mean human model.

PHZD surface corresponding to walking at two different speeds. This will allow for a smooth transition between these two walking speeds—one that respects the invariance of the PHZD surface associated to the walking at each speed.

Speed Regulation Overview. The first step in the procedure is to obtain optimal walking controller parameters by solving (HIO). By definition, these parameters, α^*, correspond to a local minima in Cost_{HD} and satisfy the constraints (C1)–(C5). The remaining steps in the process, therefore, can be viewed as perturbing and fixing v^*_{hip} and then solving an optimization problem which effectively searches in a neighborhood of α^*, subject to the same constraints (C1)–(C5). Choosing a small perturbation on v^*_{hip} and using α^* as the seed to the *speed regulation optimization* results in rapid convergence. The process is iterated using the solution to one optimization as the seed to the next until controllers for the desired maximum or minimum v_{hip} are obtained.

Walking Speed Specification. Starting with $v^0_{\text{hip}} = v^*_{\text{hip}}$, discrete walking speeds are specified via the following constraint

$$v^{l\pm1}_{\text{hip}} = v^l_{\text{hip}} \pm \delta, \tag{C6}$$

with $l \in \mathbb{Z}$ and δ the perturbation magnitude; where δ is chosen based on velocity resolution and convergence requirements (smaller δ leads to faster convergence in the following optimization).

Speed Regulation Cost. The cost function corresponding to each speed regulation step l is as follows:

$$\text{Cost}_{\text{SR}}(\alpha, \alpha^l) = \sum_{i \in \text{Output}} \int_0^T \left|\left| y^d_i(t, \alpha_i) - y^d_i(t, \alpha^l_i) \right|\right|^2 dt. \tag{34}$$

This is the integral norm of the difference between the current controller outputs, $y_d(t, \alpha)$, and the controller outputs computed via the solution to the previous speed regulation step, $y_d(t, \alpha^l)$. As the initial seed to the speed regulation procedure, $\alpha^0 = \alpha^*$, is the solution to the *human-inspired PHZD optimization*. This objective function serves to both facilitate fast convergence in the following optimization (α^* satisfies (C1)–(C5)) and maintain the human-like form of the resulting walking controller outputs (α^* corresponds to a local minima in Cost_{HD}).

Speed Regulation Optimization. The goal of the *speed regulation optimization* is to find parameters α^{l+1} that solve the following constrained optimization problem:

$$\begin{aligned} \alpha^{l+1} = \underset{\alpha \in \mathbb{R}^{46}}{\text{argmin}} \ & \text{Cost}_{\text{SR}}(\alpha, \alpha^l) \\ \text{s.t.} \ & \text{(C1)–(C6)} \end{aligned} \tag{SRO}$$

with Cost_{SR} the cost given in (34). The optimization (SRO) can be iteratively solved to obtain a set of $(v^{MAX}_{\text{hip}} - v^{MIN}_{\text{hip}})/\delta$ walking control parameters.

Extended Canonical Walking Function. It was found in [23] that to describe more complex walking motions, such as going up and down stairs, the canonical walking function must be augmented to account for the role that the environment plays on this system. Specifically, the *extended canonical walking function (ECWF)* is given by the time solution to a linear mass-spring-damper system subject to sinusoidal excitation:

$$\begin{aligned} y^e_H(t, \alpha^e_i) =& e^{-\alpha^e_{i,4} t}\left(\alpha^e_{i,1}\cos(\alpha^e_{i,2}t) + \alpha^e_{i,3}\sin(\alpha^e_{i,2}t)\right) \\ &+ \alpha^e_{i,5}\cos(\alpha^e_{i,6}t) + \kappa(\alpha)\sin(\alpha^e_{i,6}t) + \alpha^e_{i,7}, \end{aligned} \tag{35}$$

where $\kappa(\alpha^e_i) = (2\alpha^e_{i,4}\alpha^e_{i,5}\alpha^e_{i,6})/((\alpha^e_{i,4})^2 + (\alpha^e_{i,2})^2 - (\alpha^e_{i,6})^2)$ and $i \in$ Outputs. Note that due to the linearity of the parameters $\alpha^e_{i,1}$, $\alpha^e_{i,3}$, $\alpha^e_{i,5}$ and $\alpha^e_{i,7}$ in (35), we can write:

$$y^e_H(t, \alpha^e_i) = Y^e_H(t, \alpha^e_{i,2}, \alpha^e_{i,4}, \alpha^e_{i,6}) \begin{bmatrix} \alpha^e_{i,1} \\ \alpha^e_{i,3} \\ \alpha^e_{i,5} \\ \alpha^e_{i,7} \end{bmatrix} \tag{36}$$

where $Y^e_H(t, \alpha^e_i) \in \mathbb{R}^{1\times 4}$ only depends on the parameters $\alpha^e_{i,2}$, $\alpha^e_{i,4}$, $\alpha^e_{i,6}$. The CWF can naturally be written as a special case of the ECWF by, given parameters $\alpha_i \in \mathbb{R}^5$ for the CWF (4), defining $\iota_e(\alpha_i) := (\alpha_i, 0, 0)$. Through this embedding, we can therefore consider the same human-inspired controller that was considered for the CWF by replacing the CWF with the ECWF in (7). Similarly, we can

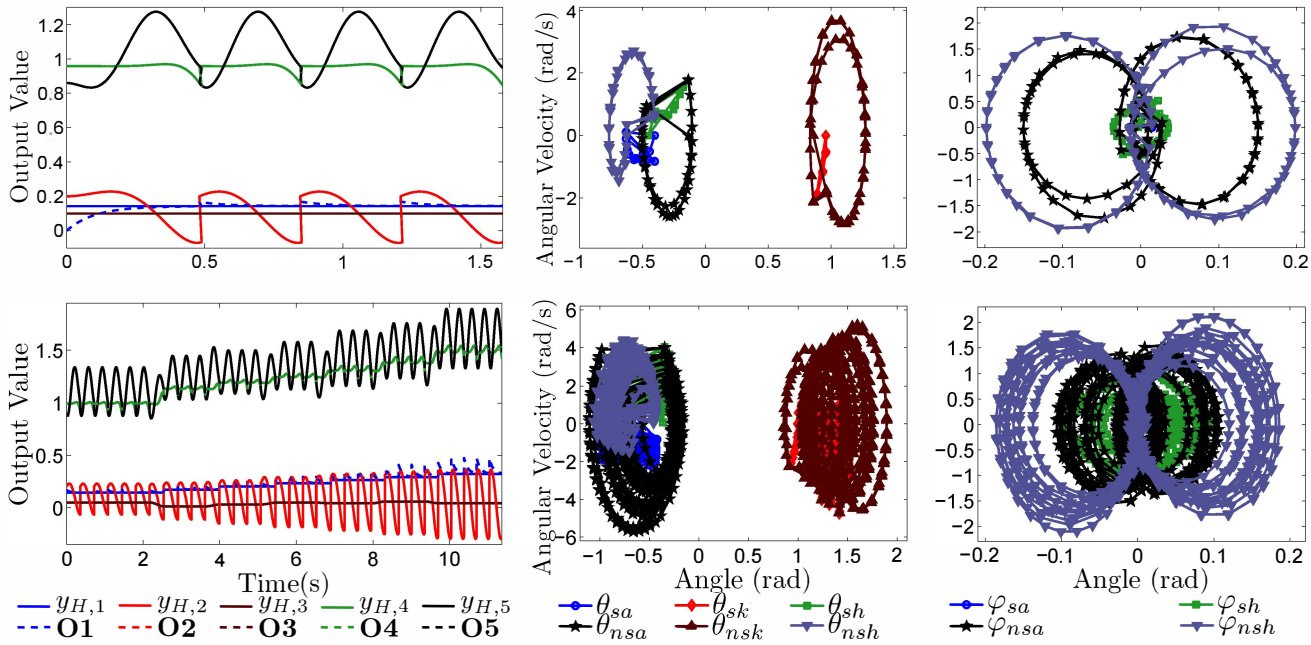

Fig. 3: Simulation results for steady-state walking starting from a perturbed fixed point (top) and speed regulation (bottom), showing controller outputs (left), phase portraits for pitch angles (middle) and roll angles (right).

consider the PHZD surface for the ECWF which we denote by: $\mathbf{PZ}_{\alpha^e}$. Finally, we note that since ξ_1 is just the linearized position of the hip, which is used to parameterize time, we can write the parameterized ECWF as $y_H^e(\xi_1, \xi_1^0, v_{\text{hip}}, \alpha_i^e) := y_H^e(\frac{\xi_1 - \xi_1^0}{v_{\text{hip}}}, \alpha_i^e)$, which is now viewed as a function of ξ_1.

Motion Transitions. The advantage to the ECWF is that, given any two PHZD surfaces these surfaces can be connected with the ECWF to ensure that partial hybrid zero dynamics is maintained, i.e., the ECWF can "glue" together any two PHZD surfaces; this is not possible with the CWF as there are not enough parameters present. To see this, let α^{l-1} and α^l be the parameters of the CWF associated with walking at two different successive speeds. Associated with these parameters are the position of the hip at the beginning and end of a step: $\xi_1^{0,l} = \delta p_{\text{hip}}(\Delta_q \vartheta(\alpha^l))$ and $\xi_1^{f,l} = \delta p_{\text{hip}}(\vartheta(\alpha^l))$. To construct a surface connecting the the PHZD surface associated with these two walking speeds, consider the ECWF at the beginning of a step associated to α^{l-1} and the end of a step associated with α^l:

$$y_i^0 = y_H^e(\xi_1^{0,l-1}, \xi_1^{0,l-1}, v_{\text{hip}}^{l-1}, \iota_e(\alpha_i^{l-1})) \quad (37)$$

$$\dot{y}_i^0 = \frac{d}{d\xi_1} y_H^e(\xi_1, \xi_1^{0,l-1}, v_{\text{hip}}^{l-1}, \iota_e(\alpha_i^{l-1}))\Big|_{\xi_1 = \xi_1^{0,l-1}} \quad (38)$$

$$y_i^f = y_H^e(\xi_1^{f,l}, \xi_1^{0,l}, v_{\text{hip}}^{l}, \iota_e(\alpha_i^{l})) \quad (39)$$

$$\dot{y}_i^f = \frac{d}{d\xi_1} y_H^e(\xi_1, \xi_1^{0,l}, v_{\text{hip}}^{l}, \iota_e(\alpha_i^{l}))\Big|_{\xi_1 = \xi_1^{f,l}} \quad (40)$$

for $i \in \text{Outputs}$.

The goal is to find a parameters, α_i^e, for the ECWF such that $\iota_e(\alpha_i^{l-1})$ and $\iota_e(\alpha_i^l)$ can be replaced by α_i^e in (37)-(40). To achieve the goal of determining the parameters α_i^e, we utilize (36) to form the following matrix:

$$\mathbb{Y} = \begin{bmatrix} Y_H^e(\xi_1^{0,l-1}, \xi_1^{0,l-1}, v_{\text{hip}}^l, \alpha_{i,2}^e, \alpha_{i,4}^e, \alpha_{i,6}^e) \\ \frac{d}{d\xi_1} Y_H^e(\xi_1, \xi_1^{0,l-1}, v_{\text{hip}}^l, \alpha_{i,2}^e, \alpha_{i,4}^e, \alpha_{i,6}^e)\Big|_{\xi_1 = \xi_1^{0,l-1}} \\ Y_H^e(\xi_1^{f,l}, \xi_1^{0,l}, v_{\text{hip}}^l, \alpha_{i,2}^e, \alpha_{i,4}^e, \alpha_{i,6}^e) \\ \frac{d}{d\xi_1} Y_H^e(\xi_1, \xi_1^{0,l}, v_{\text{hip}}^l, \alpha_{i,2}^e, \alpha_{i,4}^e, \alpha_{i,6}^e)\Big|_{\xi_1 = \xi_1^{f,l}} \end{bmatrix}$$

It is easy to verify that picking $\alpha_{i,2}^e = \alpha_{i,2}^l$, $\alpha_{i,4}^e = \alpha_{i,4}^l$ and $\alpha_{i,6}^e > 0$ results in $\mathbb{Y}$ being nonsingular. Therefore, the final four parameters of α_i^e can be determined by picking:

$$\begin{bmatrix} \alpha_{i,1}^e \\ \alpha_{i,3}^e \\ \alpha_{i,5}^e \\ \alpha_{i,7}^e \end{bmatrix} = \mathbb{Y}^{-1} \begin{bmatrix} y_i^0 \\ \dot{y}_i^0 \\ y_i^f \\ \dot{y}_i^f \end{bmatrix}$$

The end result are parameters α_i^e for $i \in \text{Outputs}$. The end result of solving for α^e in this manner is that any solution starting in $\mathbf{PZ}_{\alpha^{l-1}}$ which transitions through $\mathbf{PZ}_{\alpha^e}$ for one step will begin the subsequent step on $\mathbf{PZ}_{\alpha^l}$. In other words, we will have connected the PHZD surfaces $\mathbf{PZ}_{\alpha^{l-1}}$ and $\mathbf{PZ}_{\alpha^l}$ through $\mathbf{PZ}_{\alpha^e}$, and will therefore the control laws developed will be valid even as the robot transitions between different speeds. This will be verified through simulation and experimentally in the next section.

VI. Simulation and Experimental Results

This section presents both simulation and experimental results for walking at a constant speed and transitions between multiple walking speeds.

Simulation Results. A simulation of the hybrid system, $\mathscr{H}^R_{\alpha^*,\varepsilon}$, modeling NAO is performed in which the robot starts

on the point on the guard, $(\vartheta(\alpha^*), \dot{\vartheta}(\alpha^*))$ and is controlled via the human-inspired control law, $u_{\alpha^*,\varepsilon}$ with parameters α^* obtained through optimization (HIO) and $\varepsilon = 10$ as the control gain. The resulting periodic orbit for the pitch angles and roll angles of the system are given in Figure 3. Selected frames from one step of the simulated walking are shown in Figure 4. Furthermore, the fact that the robot can be started from rest, $(q(0), \dot{q}(0)) = (0, 0)$, and converge to the periodic orbit implies robustness of the walking (in simulation). Figure 4 also shows the angles of the biped in simulation and in the experiment described later.

To demonstrate speed regulation, a simulation was conducted using a series of controller parameters α^l determined from solving the optimization problem described above for various different choices of v_{hip} between 0.14 m/s and 0.32 m/s. Transitions increased speed by 0.03 m/s every four steps. As shown in Figure 3, the actual outputs converge to the desired controller outputs on each step.

Experimental Results. The human inspired control approach is implemented experimentally on the actual NAO robot via *pseudo-feedback control* which uses the NAO's built-in PID controller is to track the $q(t)$ trajectories from simulation. Hybrid domain switches are determined via data from the force sensors in the feet—filtering of this data to effect "debouncing" induces lag in the experimental system as compared to simulation. The simulation and experiment data are compared against one another in Figure 4, which shows that the experimental angles agree closely with the simulated angles (with minor discrepancies in θ_{sk}, θ_{tor} and φ_{sa}, which are a result of the open-loop controller). Snapshots of the experimental walking are given with the simulated gait in Figure 4.

Speed regulation is also implemented experimentally using a series of controller parameters α^l determined from solving the optimization problem described above for various different choices of v_{hip} between 0.14 m/s and 0.32 m/s. Transitions increased speed by 0.03 m/s every four steps. Without Motion Transitions, the max achievable speed is 0.23 m/s, however, with Motion Transitions computed via the extended canonical function (35), a max speed of 0.32 m/s is obtained (nearly a 50% increase in top speed!). A video of the experimental walking achieve on NAO is available online [24].

VII. Concluding Remarks

This paper presented the first steps toward defining an optimization problem that provably results in stable robotic walking in 3D through the use of human output data and controllers inspired by these data. The fundamental contribution is in the form of constraints that ensure physically realizable walking and can be enforced through solutions obtained through the low-dimensional representation given by partial hybrid zero dynamics. Speed regulation enables the rapid development of walking for a variety of speeds, and with Motion Transitions, yields experimentally realized 3D walking with NAO.

References

[1] D. J. Braun, J. E. Mitchell, and M. Goldfarb, "Actuated dynamic walking in a seven-link biped robot," *IEEE Trans. on Robotics*, vol. 17, no. 1, pp. 147–56, Feb. 2012.

[2] S. Kajita, F. Kanehiro, K. Kaneko, K. Fujiwara, K. Harada, K. Yokoi, and H. Hirukawa, "Biped walking pattern generator allowing auxiliary ZMP control," in *IEEE/RSJ Intl. Conf. on Intelligent Robots and Systems*, Beijing, Oct. 2006, pp. 2993–9.

[3] M. Vukobratović and B. Borovac, "Zero-moment point—thirty-five years of its life," *Intl. J. of Humanoid Robotics*, vol. 1, no. 1, pp. 157–73, Mar. 2005.

[4] T. McGeer, "Passive dynamic walking," *Intl. J. of Robotics Research*, vol. 9, no. 2, pp. 62–82, Apr. 1990.

[5] S. Collins, A. Ruina, R. Tedrake, and M. Wisse, "Efficient bipedal robots based on passive-dynamic walkers," *Science*, vol. 307, no. 5712, pp. 1082–1085, Feb. 2005.

[6] M. W. Spong and F. Bullo, "Controlled symmetries and passive walking," *IEEE Trans. on Automatic Control*, vol. 50, no. 7, pp. 1025–31, 2005.

[7] J. W. Grizzle, C. Chevallereau, A. D. Ames, and R. W. Sinnet, "3D bipedal robotic walking: models, feedback control, and open problems," in *IFAC Symposium on Nonlinear Control Systems*, Bologna, Sep. 2010.

[8] R. W. Sinnet and A. D. Ames, "3D bipedal walking with knees and feet: A hybrid geometric approach," in *Joint 48th IEEE Conf. on Decision and Control and 28th Chinese Control Conf.*, Shanghai, Dec. 2009, pp. 3208–13.

[9] R. W.Sinnet and A. D.Ames, "Bio-inspired feedback control of three-dimensional humanlike bipedal robots," *J. of Robotics and Mechatronics*, vol. 24, no. 4, pp. 595–601, Aug. 2012.

[10] S. Srinivasan, I. A. Raptis, and E. R. Westervelt, "Low-dimensional sagittal plane model of normal human walking," *ASME J. of Biomechanical Eng.*, vol. 130, no. 5, Oct. 2008.

[11] E. R. Westervelt, J. W. Grizzle, and D. E. Koditschek, "Hybrid zero dynamics of planar biped walkers," *IEEE Trans. on Automatic Control*, vol. 48, no. 1, pp. 42–56, 2003.

[12] E. R. Westervelt, J. W. Grizzle, and C. C. de Wit, "Switching and pi control of walking motions of planar biped walkers," *IEEE Transactions on Automatic Control*, vol. 48, pp. 308–312, 2002.

[13] P. Holmes, R. J. Full, D. E. Koditschek, and J. Guckenheimer, "The dynamics of legged locomotion: Models, analyses, and challenges," *SIAM Review*, vol. 48, no. 2, pp. 207–304, Feb. 2006.

[14] I. Mordatch, M. de Lasa, and A. Hertzmann, "Robust physics-based locomotion using low-dimensional planning," *ACM Trans. on Graphics*, vol. 29, no. 4, pp. 71:1–8, Jul. 2010.

[15] A. D. Ames, "First steps toward automatically generating bipedal robotic walking from human data," in *Robotic Motion and Control 2011*, ser. LNICS, vol. 422. Springer, 2012, pp. 89–116.

[16] A. D. Ames, E. A. Cousineau, and M. J. Powell, "Dynamically stable bipedal robotic walking with NAO via human-inspired hybrid zero dynamics," in *Hybrid Systems: Computation and Control*, Beijing, Apr. 2012, pp. 135–44.

[17] Y. Huang, Q. Wang, B. Chen, G. Xie, and L. Wang, "Modeling and gait selection of passivity-based seven-link bipeds with dynamic series of walking phases," *Robotica*, vol. 30, no. 1, pp. 39–51, Jan. 2012.

[18] R. M. Murray, Z. Li, and S. S. Sastry, *A Mathematical Introduction to Robotic Manipulation*. Boca Raton: CRC Press, 1994.

[19] Y. Hürmüzlü and D. B. Marghitu, "Rigid body collions of planar kinematic chains with multiple contact points," *Intl. J. of Robotics Research*, vol. 13, no. 1, pp. 82–92, Feb. 1994.

[20] S. S. Sastry, *Nonlinear Systems: Analysis, Stability and Control*. New York: Springer, 1999.

[21] A. D. Ames, R. Vasudevan, and R. Bajcsy, "Human-data based cost of bipedal robotic walking," in *14th Intl. Conf. on Hybrid Systems: Computation and Control*, Chicago, Apr. 2011, pp. 153–62.

[22] C. Chevallereau, G. Bessonnet, G. Abba, and Y. Aoustin, *Bipedal Robots: Modeling, Design and Walking Synthesis*. New York: Wiley-ISTE, 2009.

[23] M. J. Powell, H. Zhao, and A. D. Ames, "Motion primitives for human-inspired bipedal robotic locomotion: Walking and stair climbing," in *IEEE Intl. Conf. Robotics and Automation*, St.Paul, May 2012, pp. 543–549.

[24] "Speed regulation in 3D robotic walking through motion transitions," http://youtu.be/kLakY9rWh6Y.

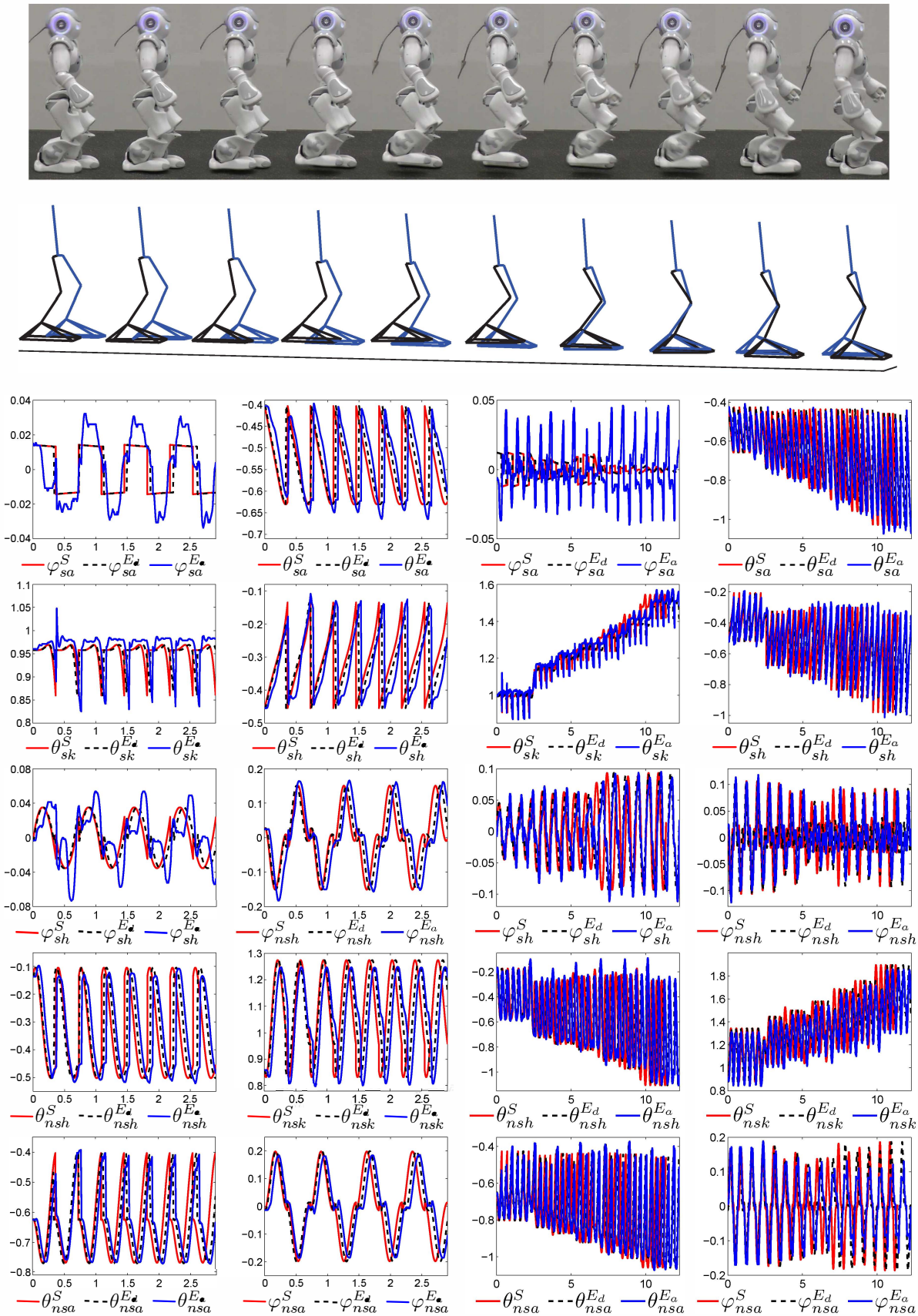

Fig. 4: Comparison of the snapshots of the actual (top row) and simulated (second row) walking gaits over one step, and experiment and simulation for steady-state walking (left two columns) and speed regulation (right two columns): X^S are from simulation, X^{E_d} are desired values from experiment, and X^{E_a} are actual values from experiment.